JES Focus Issue on Advances in Electrochemical Processes for Interconnect Fabrication in Integrated Circuits

Effects of Dimethylglyoxime and Cyclohexane Dioxime on the Electrochemical Nucleation and Growth of Cobalt

Y. Hu[1,*] **and Q. Huang**[1,2,3,**,z]

[1]*Department of Chemical and Biological Engineering, University of Alabama, Tuscaloosa, Alabama 35487, USA*
[2]*Center of Materials for Information Technology, University of Alabama, Tuscaloosa, Alabama 35487, USA*
[3]*Alabama Water Institute, University of Alabama, Tuscaloosa, Alabama 35487, USA*

Electrodeposition of cobalt on blanket Si with extremely thin cobalt seed was studied in the presence of two additives, dimethylglyoxime (DMG) and cyclohexane dioxime (CHD). Cyclic voltammetry (CV), potentiostatic current transients and galvanostatic nucleation studies were conducted to understand the effects of DMG and CHD on cobalt nucleation process. A typical cross-over in the cathodic sweep was observed in CV studies, consistent with a 3D cobalt nucleation and growth. An interesting "two-peak" phenomenon was observed in the potentiostatic studies with median concentrations of DMG and CHD. A two-step reduction reaction mechanism was proposed. The first peak was identified as the reduction reaction of Co^{2+} chelate, and the second peak was related to that of free Co^{2+}. This mechanism was further verified with the absence of the second current peak in a solution without free Co^{2+}.
 [DOI: 10.1149/2.0241901jes]

Manuscript submitted October 16, 2018; revised manuscript received November 16, 2018. Published November 30, 2018. *This paper is part of the JES Focus Issue on Advances in Electrochemical Processes for Interconnect Fabrication in Integrated Circuits.*

The scaling of damascene copper interconnects faces significant challenges in recent years because of the exponential increase of the resistivity of copper lines, particularly, for 7 nm technology and beyond.[1] The main reason for this resistivity increase is because the electron scattering at interfaces (between copper and surrounding materials) overwhelms the intrinsic electron scattering and dominates the material resistivity.[2] One of the solutions to this challenge is to replace copper with another material with a much shorter electron mean free path.[3] The resistivity of such materials will continue to be dominated by the intrinsic scattering and will not dramatically increase as the dimension decrease. Cobalt is of great interest for this application due to its short mean free path, compatibility with semiconductor manufacturing, and a relatively low material cost.[4,5]

Electrodeposition is a simple and economical way to deposit metal films. However, it requires a complete understanding of the nucleation and growth process to design the right chemistry and process for a target product. For example, the interactions between additive components in a damascene copper chemistry has to be well understood to achieve a so-called bottom-up fill.[6–12] In addition, the deposition processes also have to be finely tuned in conjunction with the chemistry to improve nucleation and minimized sidewall defects in the interconnect structures.[13] Chronoamperometry is widely used to provide insights of the nucleation process. Under a constant potential, the growth rates of nuclei are reflected in the acquired current transients.[14] This method has been used to investigate the nucleation of cobalt on different substrates such as nickel, gold,[15–17] copper,[17,18] palladium[17,19,20] and glassy carbon.[15,21–23]

On the other hand, organic additives also greatly affect the film morphology and properties.[24] Specifically, different functional groups in organic additives were found to affect the deposition process. For example, molecules with a pair of conjugated oxime groups such as DMG and CHD showed a strong suppression effect on cobalt deposition.[25,26] Thiol groups were found to accelerate the deposition and amine groups would suppress the deposition rates of iron group metals.[27–29] However, studies to investigate the influence of organic additives on the cobalt nucleation process are limited.

This paper presents a study of the effect of DMG and CHD on Co nucleation process. Since the early stage of electrodeposition of Co depends strongly on the nature of substrates, an industrially relevant material stack, physical vapor deposited (PVD) TaN and thin Co, was used as the substrate.

Experimental

Experiments were carried out in a three-compartment cell with a glass frit to separate the cathode and anode solutions. A saturated calomel electrode (SCE) was used as the reference electrode, connecting to catholyte through a capillary. All potentials were referred with respect to this SCE. Si coupons cleaved from a 12-inch blanket wafer with Co (10 nm, PVD) on TiN (5 nm, PVD) were used as cathodes. A thin Co seed was used to mimic the substrates used in industry and to provide enough conductivity for the electrodeposition studies. But the seed is not expected to be continuous and Co electrodeposition behavior is dominated by the underneath TiN layer. The area of deposition was defined with plating tape and fixed at 0.385 cm^2.

The cobalt makeup solution was adapted from our previous study,[26] containing 0.01 M $CoSO_4$, 0.1 M Na_2SO_4, 0.1 M H_3BO_3, and 0.1 g/L sodium dodecyl sulfate (SDS). The pH of Co solution was adjusted to 5.0 with H_2SO_4 and NaOH. Concentrated DMG solutions (23,000 ppm) and CHD solutions (7,000 ppm) were prepared using the corresponding sodium salts. The prepared additives were then added into the Co makeup solution up to various concentrations of DMG or CHD. Another cobalt makeup solution containing 0.4 mM $CoSO_4$, 0.1 M Na_2SO_4, 0.1 M H_3BO_3, and 0.1 g/L sodium dodecyl sulfate (SDS), pH = 5.0 was also used, where a low Co^{2+} concentration is needed to ensure the complete complexation. All salts and organic additives were at least ACS grade and deionized (DI) water with a resistivity of 18 MOhm-cm was used in all studies.

Cobalt nucleation was studied using electrochemical techniques (cyclic voltammetry, chronoamperometry and galvanostatic DC deposition). An Autolab 302N potentiostat was used for all electrochemical studies. Surface morphology of the deposited Co was examined with a scanning electron microscope (SEM, JEOL 7000, Japan).

Results

Cyclic voltammetry.—Figure 1 shows a typical cyclic voltammetry (CV) curve for cobalt deposition in the additive free makeup solution. A scan rate of 81 mV s^{-1} was used. The voltammogram started at –0.3 V, scanned in the negative direction and

*Electrochemical Society Student Member.
**Electrochemical Society Member.
[z]E-mail: qhuang@eng.ua.edu

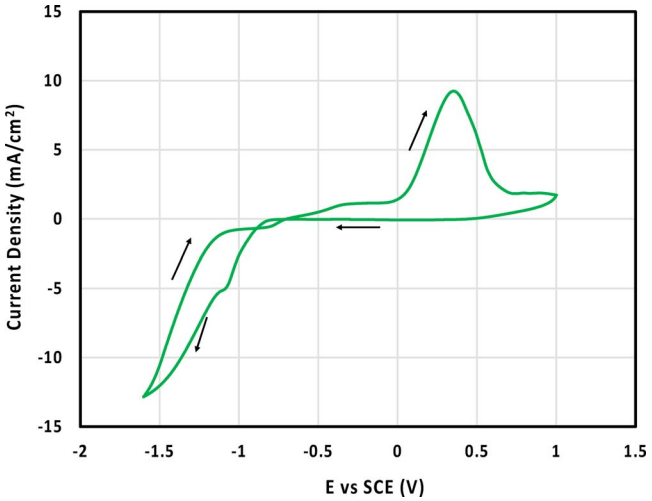

Figure 1. Cyclic voltammograms of Co deposition in aqueous solution comprising 0.01 M $CoSO_4$ + 0.1 M Na_2SO_4 + 0.1 M H_3BO_3 + 0.1 g/L SDS with pH 5.0. Potential scan rate was 81 mVs^{-1}.

reversed at –1.6V. A cross-over was observed at around –0.90V, which confirmed a typical Volmer-Weber three dimensional nucleation and growth process.[30] The sharp increase of cathodic current density observed at –0.80 V corresponded to cobalt electrodeposition, resulting a shoulder peak at –1.15 V. The further increase of current density below –1.15 V is due to water reduction. Only one intense peak was observed in the anodic sweep at potential above 0 V and it is believed to result from the dissolution of cobalt. As discussed above, Co deposition dominates the current from –0.80 V to –1.15V. Therefore, a range of different potentials between –0.80 V and –1.1 V were selected for the following potentiostaic studies on Co nucleation.

Potentiostatic current transients.—Figure 2 shows a series of current transients for the electrodeposition of cobalt at various potentials in the range of –0.85 to –1.05 V. An initial sharp decay which corresponds to an adsorption process was observed at relative less negative applied potential (–0.85 V, –0.90 V). This rapid decay is followed by a current increase due to an increase in the surface area associated with nucleus formation on the substrate. After a maximum, current density gradually decreased again upon the development of a mass transport

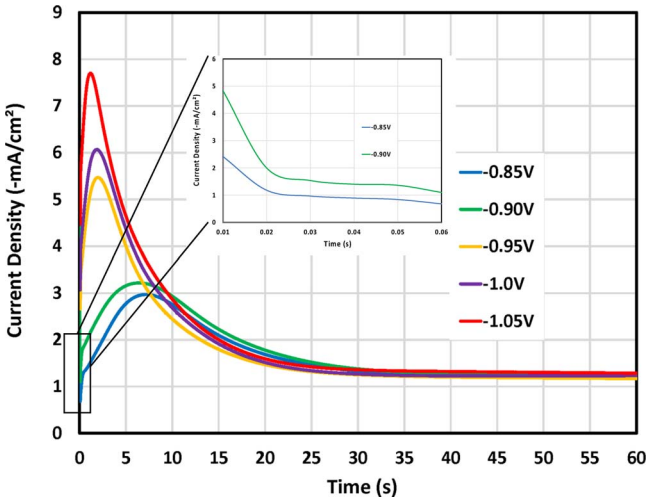

Figure 2. Family of potentiostatic current transients obtained during the electrodeposition of cobalt onto thin seed blanket wafer without additives at various potentials. The inset shows the magnified initial section of the transient curves at –0.85 and –0.90 V.

limited process. An ideal mass transport limited current decay during potentiostatic deposition can be described by the so-called Cottrell equation.[31] However, the currents in this study do not decay to 0 but stay at a constant of around 1.5 mA/cm^2. In this paper, we call this region of current transients as a "steady state current density". The observation of this steady state is believed to relate to a free convection of the electrolyte as well as a forced convection upon hydrogen evolution reaction. Since cobalt deposition occurs at a comparably negative potential, hydrogen evolution inevitably occurs. The surface agitation caused by hydrogen bubbling promotes the mass transport. The observed steady state current density includes Co deposition and hydrogen evolution.

The suppression effect of dioxime molecules including DMG and CHD on Co electrodeposition has been reported previously.[26] To further understand their impacts on the initial nucleation in Co deposition, current transients were acquired at various potentials and different additive concentrations. Figure 3 shows the chronoamperometry studies of Co nucleation in presence of DMG. The addition of 10 ppm DMG had little effects on the overall nucleation process, but a change of current peaks was observed. For example, the height of current peaks decreased (from 5.4 mA/cm^2 to 4.3 mA/cm^2) at –0.95V. Similar behavior was also observed at –1.0 V. However, an increase of current peak was seen at –1.05V. Moreover, the time to reach current peaks increased. Take –0.90 V case as an example, the time to reach the maximum current increased from around 6 s to 9 s upon the addition of 10 ppm DMG. In addition, the steady state current densities were almost the same for all potentials studied.

The suppression effect became more pronounced when the DMG concentration was increased to 100 ppm. The magnitudes of all current peaks decreased. More importantly, two nucleation peaks were observed for all applied potentials except for –0.85 V. It was noted that the height of second peak was higher than the first one. Moreover, the appearance of second peak delayed as the applied potentials became less negative. In detail, the second peak was at around 8 s, 13 s, 14 s, 28 s as the applied potential changed from –1.05 V to –0.9 V. The second peak did not fully emerge at –0.85 V up to a deposition time of 60 seconds and a steady state current was not reached. The steady state current densities at other potentials were approximately the same as the additive free and the 10 ppm DMG cases, suggesting the hydrogen evolution reaction rates were not significantly changed in the presence of 100 ppm DMG.

The height of the first peak significantly increased with the addition of 300 ppm DMG. Take –1.0 V as an example, the magnitude of first current peak increased from 2.8 mA/cm^2 for 100 ppm DMG to 4.2 mA/cm^2 for 300 ppm. The second peak was only observed at relatively more negative applied potentials (–1.0 and –1.05 V). Furthermore, the appearance of the second peak further delayed and the height of second peak declined. Take –1.05 V as an example, the second peak showed up nearly 17 s later than the case with 100 ppm DMG. Moreover, the height of second peak dropped from 5.1 mA/cm^2 to 3.5 mA/cm^2. In addition, the steady state current density not only increased along with the applied potential in presence of 300 ppm DMG but also were higher than 100 ppm DMG cases at any potential studied. At a higher DMG concentration of 500 ppm, such trends became even more pronounced. The height of first peak decreased and the second current peak further delayed and diminished. In addition, it is worth noting that no significant difference was observed for the current transients at –0.85, –0.90, and –0.95 V, including the steady state current densities.

The effect of CHD on Co nucleation was studied in the same fashion. Due to a stronger suppression effect of CHD than DMG, a more negative potential range of –0.90 V to –1.1 V was used for the studies. Figure 4 presents the chronoamperometry study of Co nucleation. The suppression effect and the second current peak were clearly seen with the addition of 10 ppm CHD. The height of the first peak was lower than the second one, which was the same as 100 ppm DMG. Furthermore, the appearance of second peak delayed when a less negative potential was applied. For example, the second peak shifted from 3 s to 10 s as the applied potential changed from

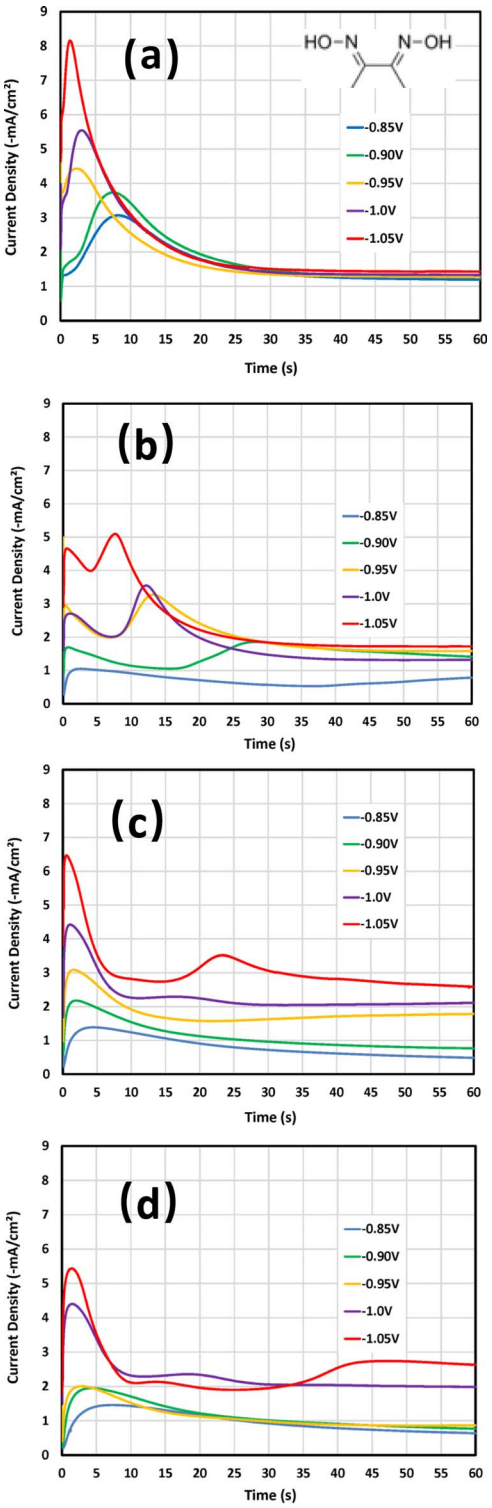

Figure 3. Current transients for cobalt deposition on thin Co seed blanket wafer at different potentials in 0.01M Co solutions with (a) 10-ppm (b) 100-ppm (c) 300-ppm (d) 500-ppm DMG. Inset in (a) shows the molecular structure of DMG.

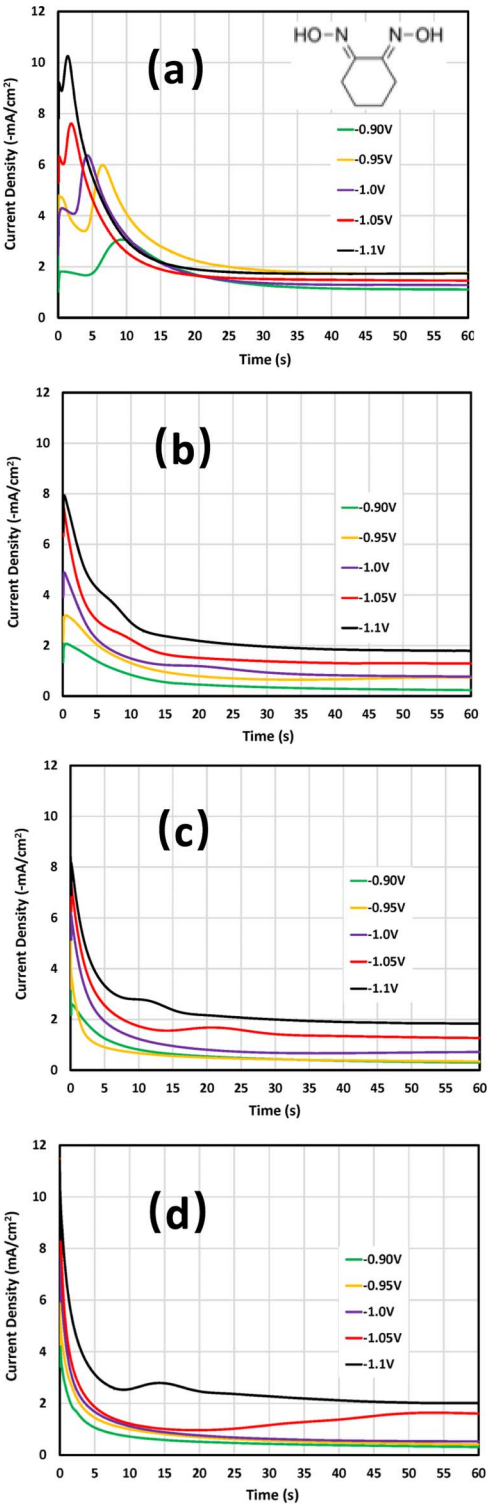

Figure 4. Current density –time transients for cobalt deposition on thin Co seed blanket wafer at different potentials in 0.01M Co solutions with (a) 10-ppm (b) 100-ppm (c) 300-ppm (d) 500-ppm CHD. Inset in (a) shows the molecular structure of CHD.

–0.90 V to –1.1 V. The effects of higher concentrations of CHD followed the same trend as DMG in Figure 3. The appearance of the second peak delayed and the peak height decreased as the CHD concentration increased. However, the first current peaks were found to be much sharper with CHD than DMG. No rising part of current was observed in most of the cases, resulting in a current decay instead of a current peak at the beginning of a transient.

Galvanostatic deposition with different current densities of –2, –4 and –10 mA/cm^2 were used to examine the effects of DMG and CHD on Co deposition. A constant charge density of –6.5 mC/cm^2 was used. The deposition time needed for this charge density are only up to 3.2 seconds, corresponding to a very small section at the beginning of current transients shown in Figures 3 and 4. Figures 5 and 6 show the top down SEM images of deposits. The same image of the

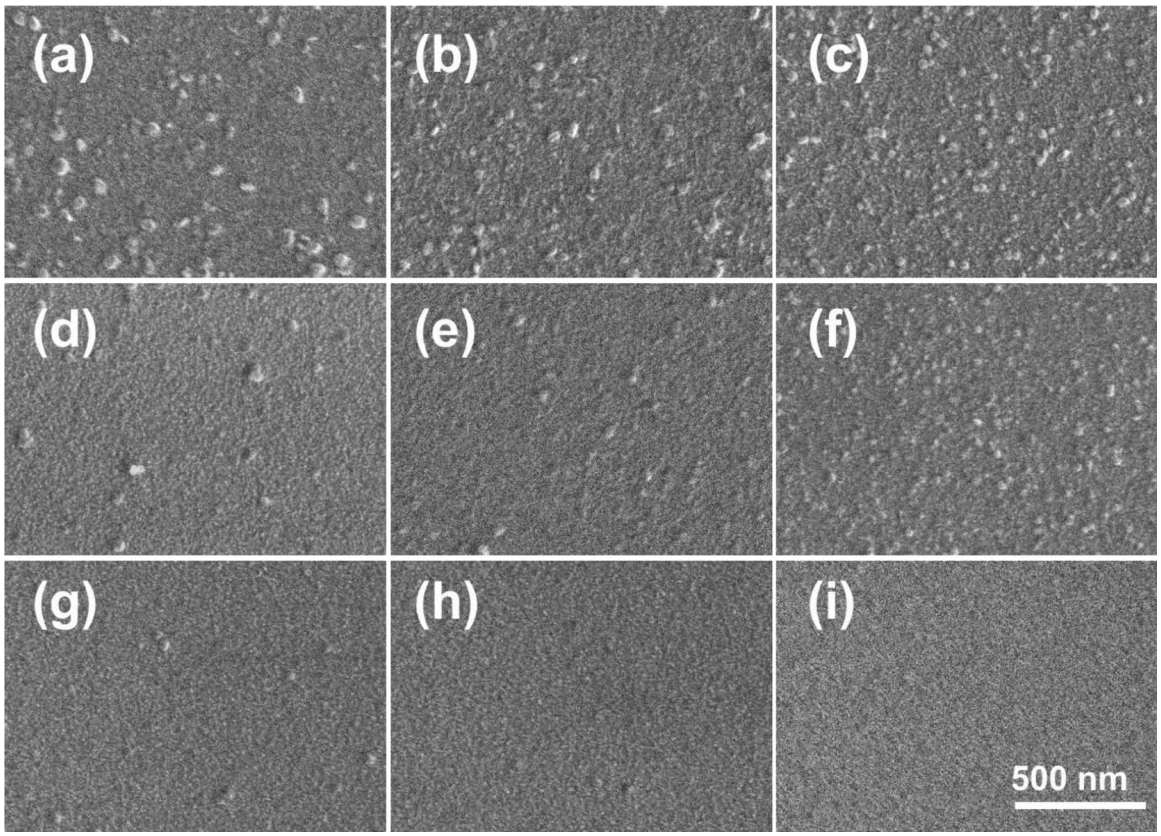

Figure 5. SEM images of cobalt nuclei deposited thin Co seed blanket wafer from solution containing 0.01 M Co with (a-c) 0, (d-f) 10, and (g-i) 100 ppm DMG at (a,d,g) –2, (b,e,h) –4, and (c,f,i) –10 mA/cm^2. different concentration of DMG and different current densities. The total deposition charge was –6.5 mC/cm^2.

substrate before deposition was included for comparison. It was evident that the nucleation density increased and the nucleus size decreased as the current densities increased in the additive free electrolyte. The addition of 10 ppm DMG resulted in a decrease in the number of cobalt nuclei for all the current densities used. Moreover, this decrease was the most pronounced at –4 mA/cm^2 and the least at –10 mA/cm^2. The nucleation density further decreased as the DMG concentration increased to 100 ppm. While this decrease of nucleation density was very evident at –2 mA/cm^2, only a handful of cobalt nuclei was observed at –4 and –10 mA/cm^2.

A more pronounced suppression effect on nucleation was observed with the addition of CHD. The cobalt nucleation density and size with 10 ppm CHD were similar to the case with 100 ppm DMG. This is consistent with the similarity in the double peak current transients

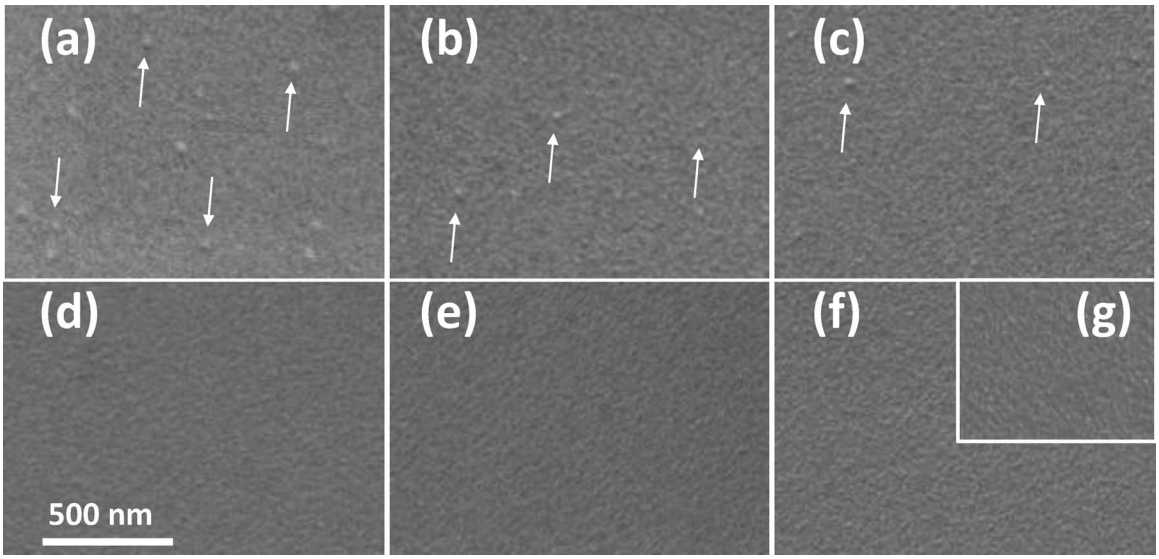

Figure 6. SEM images of cobalt nuclei deposited thin Co seed blanket wafer from solution containing 0.01 M Co with (a-c) 10 and (d-f) 100 ppm CHD at (a,d) –2, (b,e) –4, and (c,f) –10 mA/cm^2. The total charge was –6.5 mC/cm^2. The blanket substrate was shown in (g). White arrows were used to point at a few example nuclei.

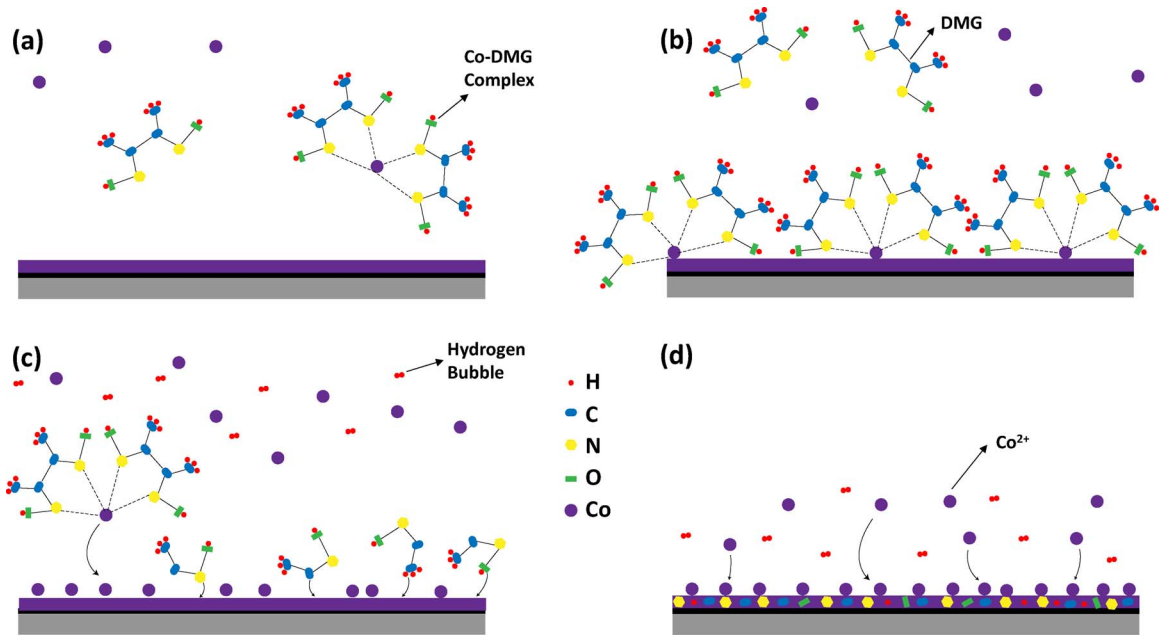

Figure 7. Diagrams showing the proposed two-step nucleation mechanism. (a) The solution contains Co^{2+}, DMG, and $Co(DMG)_2$ complex before reaction. (b) The adsorption of $Co(DMG)_2$ complex is stronger than Co^{2+}, and it preferably adsorbs on the electrode and prevents the adsorption of free Co^{2+} (c) Co^{2+} chelates reduction happens accompanying the hydrogen evolution reaction, which corresponds to the first current peak. (d) Co^{2+} reduction reaction happens accompanying the hydrogen evolution reaction, which corresponds to the second current peak. The reduction of $Co(DMG)_2$ results in a breakdown of suppression, incorporates organic fragments or elements into the film, and frees up electrode surface.

observed in these two cases. There were very few cobalt nuclei observed at –4 and –10 mA/cm^2 when 10 ppm CHD was added into the solution. More cobalt nuclei were deposited at –2 mA/cm^2, but they are much less and smaller compared with the additive-free case. Increasing CHD concentration to 100 ppm led to no cobalt nuclei observed under SEM for all the current densities used.

To summarize the results, several interesting phenomena were observed: *i)* two current peaks were observed with the addition of median to low concentrations of DMG or CHD; *ii)* the height of first peak rises and the second peak diminishes upon the further addition of DMG or CHD; *iii)* the appearance of second peak delayed as the concentrations of DMG or CHD increase; *iv)* the addition of DMG or CHD suppressed the formation of cobalt nuclei dramatically, and this suppression was more pronounced for CHD than DMG at a same concentration.

Discussion

It is known that current transients reflect the physical and chemical changes during electrochemical nucleation process. In this study, several reactions are believed to occur simultaneously during the nucleation process and should be included in the discussion: Co^{2+} reduction reaction, Co^{2+} chelates reduction reaction, and hydrogen evolution reaction.

$$Co^{2+} + 2e \rightarrow Co \quad [1]$$

$$Co^{2+} + 2L^{-} \rightarrow CoL_2 \quad [2]$$

$$CoL_2 + 2e \rightarrow Co + 2L^{-} \quad [3]$$

$$2H^{+} + 2e \rightarrow H_2 \quad [4]$$

$$2H_2O + 2e \rightarrow H_2 + 2OH^{-} \quad [5]$$

where L stands for a ligand, and CoL_2 for a Co chelate consisting of one Co^{2+} and two dioxime molecules. While the above equations are used to represent the reduction reactions in solution, the detailed mechanisms can involve adsorbed intermediates. For example, the electrodeposition of iron group metals, namely, Ni, Fe, and Co, typically involves a monovalent metal cation intermediate species adsorbed on the electrode surface.[32–35]

$$Co^{2+} + OH^{-} + e^{-} \rightarrow CoOH_{ads} \quad [6]$$

$$CoOH_{ads} + e^{-} \rightarrow Co + OH^{-} \quad [7]$$

Electrochemical nucleation and growth of metal on a foreign substrate have been extensively studied.[36–38] A 3D nucleation process can be typically characterized with a single current peak in the transient experiment. This single-peak current transient curve results from a synergistic interaction between a preferred deposition of metal on itself, the increase of total surface area of metal nuclei, and a consumption and depletion of metal cations in the solution in the vicinity of nuclei. Such a current peak has also been reported for Co deposition. However, for many cases in our studies, two current peaks were observed during the potentiostatic nucleation process. It is highly likely that two reactions happen separately and result in these two peaks. Attempts are made here to discuss the mechanisms for such a new nucleation behavior.

Proposed mechanism.—Figure 7 shows a diagram illustrating the proposed mechanism for the Co electrodeposition in a DMG-containing electrolyte. Initially, the Co solution contains Co^{2+} and $Co(DMG)_2$ complex before deposition. All the DMG molecules are present in the form of $CO(DMG)_2$ complex due to an extremely high stability constant of the complex and a much higher concentration of Co^{2+} than DMG.[39] A previous study[26] showed that the suppression effect of dioxime molecules on Co electrodeposition broke down at a potential closely related to the stability constants of Co-dioxime chelates. This suggests that the suppression effect results from a preferred adsorption of such chelates over Co^{2+} and the suppression breaks down because of the reduction of the chelate

at more negative potentials. With a stronger electro-adsorption of $Co(DMG)_2$ than Co^{2+}, the former is expected to preferably adsorb on the electrode and prevent the adsorption of CoOH intermediate. In other words, the electrode is occupied by $Co(DMG)_2$ complex. After that, the $Co(DMG)_2$ on the surface complex will be reduced to Co metal when a sufficiently negative potential is applied. Upon the commence of deposition, the adsorbed $Co(DMG)_2$ complex would get incorporated into the Co film and the electrode surface is freed up. Such incorporation has been verified with second ion mass spectroscopy analysis (not shown here), where the carbon and cyanide impurity concentrations increased for about 5 and 20 times, respectively, upon the addition of DMG into electrolyte. The cyanide species is a direct measurement of nitrogen in Co film due to DMG incorporation. While the electrode surface is freed up upon $Co(DMG)_2$ reduction and DMG incorporation, $Co(DMG)_2$ complex in electrolyte would preferably take up the empty active site, resulting a continuous reduction reaction of Co^{2+} chelates. Because the reduction potential of $Co(DMG)_2$ to Co metal is more negative than that of H^+ to H_2, the hydrogen evolution reaction inevitably occurs at the same time. In fact, the Co-dioxime chelate has been found a catalyst for hydrogen evolution reaction.[40] The combination of these two reactions corresponds to the first current peak in potentiostatic nucleation. As the chelate reduction (Reaction 3) continues, the chelate concentration in the vicinity of electrode decreases and the surface coverage of $Co(DMG)_2$ decreases. CoOH intermediate would eventually adsorb on the electrode upon the depletion of $Co(DMG)_2$ in solution. Subsequently, both the reduction of free Co^{2+} (Reaction 1) and hydrogen evolution (Reactions 4 and 5) would occur, resulting in the second nucleation current peak.

All the observations in this study can be explained with this proposed mechanism. Take DMG as an example, the concentration of $Co(DMG)_2$ complex in solution is pretty low when DMG concentration is 10 ppm (0.086 mM). Although the $Co(DMG)_2$ chelates reduction reaction occurs, its concentration is extremely low. Depletion of chelate in solution occurs soon after chelate reduction. The surface coverage of chelate is low and the impact on the reduction of free cation (Reactions 6 and 7) are believed to be minimal. The CoOH intermediate would take up most active sites and the current peak is mainly due to Co^{2+} reduction reaction. The concentration of $Co(DMG)_2$ complexes further increases upon the addition of 100 ppm (0.86 mM) DMG into the solution. The $Co(DMG)_2$ reduction reaction and hydrogen evolution reaction are strong enough to be seen as the first peak. In addition, it takes longer time to deplete the chelate in the vicinity of electrode and free up the surface for the reduction of free Co^{2+}, resulting in a delay of the second nucleation current peak. More $Co(DMG)_2$ complexes are formed with the addition of 300 ppm (2.58 mM) DMG. The height of the first peak rises due to a high concentration of $Co(DMG)_2$ complexes and a higher hydrogen evolution reaction rate. On the other hand, the second current peak did not emerge up to 60 seconds at less negative potentials. At a high concentration of $Co(DMG)_2$, the complex in electrolyte would immediately adsorb on an active site on the electrode surface once such a site is freed up upon the reduction of an adsorbed chelate. Because the chelate reduction rate is slower at a less negative applied potential, it takes longer time to deplete $Co(DMG)_2$ complexes in the solution and it would take longer time than 60 seconds for the second current peak to evolve.

The same explanation can also be applied to the CHD studies. In this case, a much higher stability constant of $Co(CHD)_2$ than $Co(DMG)_2$ predicts a slower reduction of the adsorbed chelate at a same applied potential.[39] This translates to a slower depletion of the $Co(CHD)_2$ complex in the solution in the vicinity of electrode. Therefore, the $Co(CHD)_2$ chelates reduction reaction and hydrogen evolution reaction were observed as the first peak even at a lower concentration, 10 ppm (0.089 mM) CHD. The stronger suppression effect of CHD than DMG also resulted in a much more negative potential required for the chelate reduction and, therefore, a much lower current efficiency of Co deposition and a much lower cobalt nuclear density in galvanostatic nucleation.

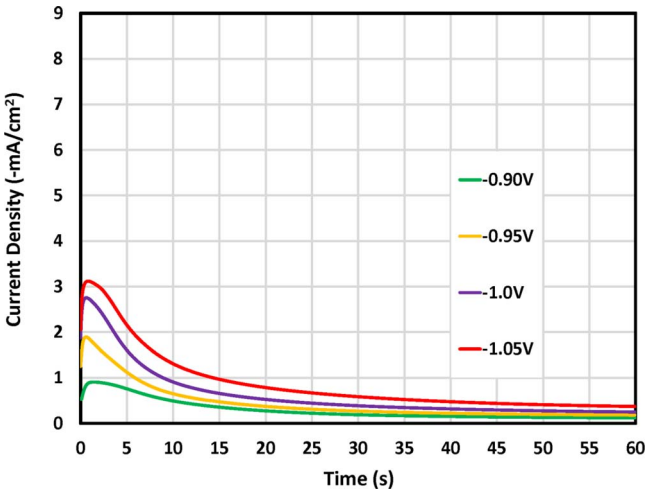

Figure 8. Current density – time transients for cobalt deposition on thin Co seed blanket wafer at different potentials with 0.4 mM Co and 100 ppm DMG in the solution.

A further discussion is provided here to validate the assignments of current peaks. The concentration of free Co^{2+} decreases and those of $Co(DMG)_2$ or $Co(CHD)_2$ complexes increase with the further addition of DMG or CHD. If free Co^{2+} reduction were assumed to result in the first current peak and chelate reduction as the second peak, the appearance of the second peak would have shifted earlier with the further addition of DMG or CHD as the time required to deplete free Co^{2+} would have decreased. This is however opposite to the observations.

Hydrogen evolution occurs inevitably throughout the nucleation studies and contributes to the current observed therein. However, it is believed that the hydrogen evolution itself does not result in a stand-alone current peak. If the second peak were solely due to hydrogen evolution reaction, the hydrogen evolution reaction would have been more pronounced when more DMG or CHD was added since $Co(DMG)_2$ and $Co(CHD)_2$ complexes are catalysts for hydrogen evolution reaction. However, this is in contradictory with the observation in Figures 3c–3d. On the other hand, a dilemma is also encountered when the first peak is assigned to the hydrogen evolution reaction. If the first peak represented the hydrogen evolution reaction, the second peak would have been cobalt nucleation reaction, including the reduction of free Co^{2+} or chelates. Since the required potential for hydrogen evolution reaction is more positive than Co deposition, the only peak observed in 10 ppm (0.086 mM) DMG cases in Figure 3a should correspond to hydrogen evolution reaction. However, SEM images from galvanostatic study in Figures 5d–5f clearly show that cobalt deposition occurs at various current densities for a small total charge, which corresponds to a deposition time well before the emerge of the only current peak in Figure 3a. Therefore, the hydrogen evolution reaction alone does not result in any of two current peaks whilst it occurs simultaneously with cobalt nucleation.

Controlled experiment.—The proposed mechanism was further confirmed with a control experiment, where 0.4 mM Co and 100 ppm (0.86 mM) DMG were used. In this study, no free Co^{2+} was expected to be present in the electrolyte because each Co^{2+} ion complexes with two DMG molecules,[41] forming a stable $Co(DMG)_2$ chelate. Figure 8 shows the current transients of the controlled experiments. Only one current peak was observed across all the potentials studied, corresponding to the first current peak in the two-peak cases in Figure 3. This current peak corresponds to the combination of Co^{2+} chelates

reduction and hydrogen evolution, consistent with the proposed mechanism and the absence of free Co^{2+} cations.

Conclusions

The effects of DMG and CHD on cobalt nucleation process were studied on TaN substrate with extremely thin Co seed. CV study showed a typical 3D nucleation process controlled by hemispheric diffusion toward the nucleation centers. Potentiostatic studies showed several new findings: *i)* two current peaks were observed with the addition of DMG or CHD; *ii)* the height of first peak rises and the second peak diminishes upon the further addition of DMG or CHD; *iii)* the appearance of second peak delayed as the concentrations of DMG or CHD increase; *iv)* the addition of DMG or CHD suppressed the formation of cobalt nuclei dramatically. A two-step nucleation mechanism was proposed, involving i) a competitive surface adsorption between Co-dioxime chelate and monovalent Co intermediate, and ii) an incorporation of adsorbed chelate upon deposition and a release of surface adsorption site. The first current peak was therefore identified as the nucleation upon Co-dioxime chelate reduction, and the second peak as nucleation current from free Co^{2+} reduction. This mechanism was further confirmed with a controlled experiment, where only the first current peak was observed with all Co^{2+} being present as the chelate. Galvanostatic DC deposition showed that CHD has stronger suppression effect on Co nucleation than DMG.

Acknowledgments

National Science Foundation is acknowledged for support through grant CMMI –1662332. YH thanks the Graduate Council at University of Alabama for a fellowship support. Brett Baker-O'Neal at SUNY Polytech and Ahmed Shafaat at GlobalFoundries are acknowledged for providing the Co seed substrates for the studies. Central analytical facility at the University of Alabama is acknowledged for the access of equipment for characterization.

ORCID

Q. Huang https://orcid.org/0000-0002-1391-6531

References

1. W. Steinhögl, G. Schindler, G. Steinlesberger, and M. Engelhardt, "Size-dependent resistivity of metallic wires in the mesoscopic range." *Physical Review B*, **66**(7), 075414 (2002).
2. W. Wu, S. Brongersma, M. Van Hove, and K. Maex, "Influence of surface and grain-boundary scattering on the resistivity of copper in reduced dimensions." *Applied physics letters*, **84**(15), 2838 (2004).
3. W. Zhang, S. H. Brongersma, O. Richard, B. Brijs, R. Palmans, L. Froyen, and K. Maex, "Influence of the electron mean free path on the resistivity of thin metal films." *Microelectronic Engineering*, **76**(1–4), 146 (2004).
4. C.-C. Wei, E. Chou, S. Shih, and S.-M. Lin, In *Bottom-up Filling of Damascene Trenches with Cobalt By Electroplating Process*, Meeting Abstracts, The Electrochemical Society: 2015; pp. 949.
5. J. Kelly, J.-C. Chen, H. Huang, C. Hu, E. Liniger, R. Patlolla, B. Peethala, P. Adusumilli, H. Shobha, and T. Nogami, In *Experimental study of nanoscale Co damascene BEOL interconnect structures*, *Interconnect Technology Conference/Advanced Metallization Conference (IITC/AMC)*, 2016 IEEE International, IEEE: 2016; pp 40.
6. A. C. West, S. Mayer, and J. Reid, "A superfilling model that predicts bump formation." *Electrochemical and Solid-State Letters*, **4**(7), C50 (2001).
7. T. Moffat, D. Wheeler, W. Huber, and D. Josell, "Superconformal electrodeposition of copper." *Electrochemical and Solid-State Letters*, **4**(4), C26 (2001).
8. T. P. Moffat, D. Wheeler, and D. Josell, "Electrodeposition of copper in the SPS-PEG-Cl additive system I. Kinetic measurements: Influence of SPS." *Journal of The Electrochemical Society*, **151**(4), C262 (2004).
9. R. Akolkar and U. Landau, "A time-dependent transport-kinetics model for additive interactions in copper interconnect metallization." *Journal of The Electrochemical Society*, **151**(11), C702 (2004).
10. P. M. Vereecken, R. A. Binstead, H. Deligianni, and P. C. Andricacos, "The chemistry of additives in damascene copper plating." *IBM Journal of Research and Development*, **49**(1), 3 (2005).
11. J. W. Gallaway and A. C. West, "PEG, PPG, and their triblock copolymers as suppressors in copper electroplating." *Journal of The Electrochemical Society*, **155**(10), D632 (2008).
12. J. W. Gallaway, M. J. Willey, and A. C. West, "Copper filling of 100 nm trenches using PEG, PPG, and a triblock copolymer as plating suppressors." *Journal of The Electrochemical Society*, **156**(8), D287 (2009).
13. S. Ahmed, Q. Huang, T. J. Cheng, P. Findeis, D. R. Koli, C. N. Troung, and S. Grunow, In *Damascene Copper Plating Recipe Engineering for Defectivity, Health of Line (HOL) and Reliability Improvement*, Meeting Abstracts, The Electrochemical Society: 2016; pp. 1909.
14. G. Oskam, J. Long, A. Natarajan, and P. Searson, "Electrochemical deposition of metals onto silicon." *Journal of Physics D: Applied Physics*, **31**(16), 1927 (1998).
15. A. Correia, S. Machado, and L. Avaca, "Direct observation of overlapping of growth centres in Ni and Co electrocrystallisation using atomic force microscopy." *Journal of Electroanalytical Chemistry*, **488**(2), 110 (2000).
16. J. Bubendorff, C. Meny, E. Beaurepaire, P. Panissod, and J. Bucher, "Electrodeposited cobalt films: hcp versus fcc nanostructuring and magnetic properties." *The European Physical Journal B-Condensed Matter and Complex Systems*, **17**(4), 635 (2000).
17. A. Sahari, A. Azizi, N. Fenineche, G. Schmerber, and A. Dinia, "Electrochemical study of cobalt nucleation mechanisms on different metallic substrates." *Materials Chemistry and Physics*, **108**(2–3), 345 (2008).
18. U. Ramsperger, A. Vaterlaus, P. Pfaeffli, U. Maier, and D. Pescia, "Growth of Co on a stepped and on a flat Cu (001) surface." *Physical Review B*, **53**(12), 8001 (1996).
19. A. Azizi, A. Sahari, M. Felloussia, G. Schmerber, C. Mény, and A. Dinia, "Growth and properties of electrodeposited cobalt films on Pt/Si (1 0 0) surface." *Applied surface science*, **228**(1–4), 320 (2004).
20. L. H. Mendoza-Huizar and C. Rios-Reyes, "Cobalt electrodeposition on polycrystalline palladium. Influence of temperature on kinetic parameters." *Journal of Solid State Electrochemistry*, **16**(9), 2899 (2012).
21. E. Gomez, M. Marin, F. Sanz, and E. Valles, "Nano-and micrometric approaches to cobalt electrodeposition on carbon substrates." *Journal of Electroanalytical Chemistry*, **422**(1–2), 139 (1997).
22. A. Soto, E. Arce, M. Palomar-Pardave, and I. Gonzalez, "Electrochemical nucleation of cobalt onto glassy carbon electrode from ammonium chloride solutions." *Electrochimica Acta*, **41**(16), 2647 (1996).
23. M. Palomar-Pardavé, I. González, A. B. Soto, and E. M. Arce, "Influence of the coordination sphere on the mechanism of cobalt nucleation onto glassy carbon." *Journal of Electroanalytical Chemistry*, **443**(1), 125 (1998).
24. M. Quinet, F. Lallemand, L. Ricq, J. Y. Hihn, P. Delobelle, C. Arnould, and Z. Mekhalif, "Influence of organic additives on the initial stages of copper electrodeposition on polycrystalline platinum." *Electrochimica Acta*, **54**(5), 1529 (2009).
25. Q. Huang, T. Lyons, and W. Sides, "Electrodeposition of Cobalt for Interconnect Application: Effect of Dimethylglyoxime." *Journal of The Electrochemical Society*, **163**(13), D715 (2016).
26. T. Lyons and Q. Huang, "Effects of Cyclohexane-Monoxime and Dioxime on the Electrodeposition of Cobalt." *Electrochimica Acta*, **245**, 309 (2017).
27. D. Liang, J. Liu, K. Reuter, B. Baker-O'Neal, and Q. Huang, "Electroplating of Fe-Rich NiFe alloys in Sub-50 nm lines." *Journal of The Electrochemical Society*, **161**(5), D301 (2014).
28. C. H. Lee, J. E. Bonevich, J. E. Davies, and T. P. Moffat, "Superconformal Electrodeposition of Co and Co–Fe Alloys Using 2-Mercapto-5-benzimidazolesulfonic Acid." *Journal of The Electrochemical Society*, **156**(8), D301 (2009).
29. X. Zheng, Y.-N. Shi, and K. Lu, "The Combination Addition of 2-Mercapto-5-benzimidazolesulfonic Acid and Thiourea to Watts Bath in Controllable Electro-Healing Cracks in Nickel." *Journal of The Electrochemical Society*, **163**(8), D349 (2016).
30. K. Oura, M. Katayama, A. Zotov, V. Lifshits, and A. Saranin, Elementary Processes at Surfaces I. Adsorption and Desorption. In *Surface Science*, Springer: 2003; pp 295.
31. F. G. Cottrell, "Der Reststrom bei galvanischer Polarisation, betrachtet als ein Diffusionsproblem." *Zeitschrift für Physikalische Chemie*, **42**(1), 385 (1903).
32. M. Jeffrey, W. Choo, and P. Breuer, "The effect of additives and impurities on the cobalt electrowinning process." *Minerals Engineering*, **13**(12), 1231 (2000).
33. H. Deligianni and L. T. Romankiw, "In situ surface pH measurement during electrolysis using a rotating pH electrode." *IBM Journal of Research and Development*, **37**(2), 85 (1993).
34. S. Hessami and C. W. Tobias, "A Mathematical Model for Anomalous Codeposition of Nickel-Iron on a Rotating Disk Electrode." *Journal of the Electrochemical Society*, **136**(12), 3611 (1989).
35. D. Gangasingh and J. B. Talbot, "Anomalous Electrodeposition of Nickel-Iron." *Journal of the Electrochemical Society*, **138**(12), 3605 (1991).
36. A. Radisic, A. C. West, and P. C. Searson, "Influence of additives on nucleation and growth of copper on n-Si (111) from acidic sulfate solutions." *Journal of the Electrochemical Society*, **149**(2), C94 (2002).
37. Q. Huang, H. Deligianni, and L. Romankiw, "Electrodeposition of gold on silicon nucleation and growth phenomena." *Journal of The Electrochemical Society*, **153**(5), C332 (2006).
38. C. Ramírez, E. M. Arce, M. Romero-Romo, and M. Palomar-Pardavé, "The effect of temperature on the kinetics and mechanism of silver electrodeposition." *Solid State Ionics*, **169**(1–4), 81 (2004).
39. A. E. Martell and R. M. Smith, *Critical stability constants*, Springer: 1974; Vol. **1**.
40. P.-A. Jacques, V. Artero, J. Pécaut, and M. Fontecave, "Cobalt and nickel diimine-dioxime complexes as molecular electrocatalysts for hydrogen evolution with low overvoltages." *Proceedings of the National Academy of Sciences*, **106**(49), 20627 (2009).
41. F. Ma, D. Jagner, and L. Renman, "Mechanism for the electrochemical stripping reduction of the nickel and cobalt dimethylglyoxime complexes." *Analytical chemistry*, **69**(9), 1782 (1997).